NEOPLASIA
www.neoplasia.com

Volume 19 Number 9 September 2017 pp. 695–706 695

# The Volume of Three-Dimensional Cultures of Cancer Cells *In Vitro* Influences Transcriptional Profile Differences and Similarities with Monolayer Cultures and Xenografted Tumors

**Erwin R. Boghaert[*], Xin Lu[†], Paul E. Hessler[†], Thomas P. McGonigal[*], Anatol Oleksijew[*], Michael J. Mitten[*], Kelly Foster-Duke[*], Jonathan A. Hickson[*], Vitor E. Santo[‡,§], Catarina Brito[‡,§], Tamar Uziel[†] and Kedar S. Vaidya[*]**

[*]In Vivo Pharmacology, Oncology Discovery, AbbVie, North Chicago, IL 60064, USA; [†]Translational Oncology, Oncology Discovery, AbbVie, North Chicago, IL 60064, USA; [‡]iBET, Instituto de Biologia Experimental e Tecnológica, Apartado 12, 2780-901 Oeiras, Portugal; [§]Instituto de Tecnologia Química e Biológica António Xavier, Universidade Nova de Lisboa, Av. da República, 2780-157 Oeiras, Portugal

## Abstract

Improving the congruity of preclinical models with cancer as it is manifested in humans is a potential way to mitigate the high attrition rate of new cancer therapies in the clinic. In this regard, three-dimensional (3D) tumor cultures *in vitro* have recently regained interest as they have been acclaimed to have higher similarity to tumors *in vivo* than to cells grown in monolayers (2D). To identify cancer functions that are active in 3D rather than in 2D cultures, we compared the transcriptional profiles (TPs) of two non-small cell lung carcinoma cell lines, NCI-H1650 and EBC-1 grown in both conditions to the TP of xenografted tumors. Because confluence, diameter or volume can hypothetically alter TPs, we made intra- and inter-culture comparisons using samples with defined dimensions. As projected by Ingenuity Pathway Analysis (IPA), a limited number of signal transduction pathways operational *in vivo* were better represented by 3D than by 2D cultures *in vitro*. Growth of 2D and 3D cultures as well as xenografts induced major changes in the TPs of these 3 modes of culturing. Alterations of transcriptional network activation that were predicted to evolve similarly during progression of 3D cultures and xenografts involved the following functions: hypoxia, proliferation, cell cycle progression, angiogenesis, cell adhesion, and interleukin activation. Direct comparison of TPs of 3D cultures and xenografts to monolayer cultures yielded up-regulation of networks involved in hypoxia, TGF and Wnt signaling as well as regulation of epithelial mesenchymal transition. Differences in TP of 2D and 3D cancer cell cultures are subject to progression of the cultures. The emulation of the predicted cell functions *in vivo* is therefore not only determined by the type of culture *in vitro* but also by the confluence or diameter of the 2D or 3D cultures, respectively. Consequently, the successful implementation of 3D models will require phenotypic characterization to verify the relevance of applying these models for drug development.

*Neoplasia (2017) 19, 695–706*

## Introduction

The prognosis of non-small cell lung cancer (NSCLC) has improved during the last decennia due to enhanced diagnostics and administration of cytoreductive and targeted therapeutics [1]. Nonetheless, the American Cancer Society estimated that in 2016 more than 220,000 men and women were diagnosed with lung cancer and more than 158,000 of them will succumb to the disease [2]. With

Abbreviation: TP, transcriptional profile.

Address all correspondence to: Kedar S. Vaidya, *In Vivo* Pharmacology, Oncology Discovery, AbbVie Inc., 1 N Waukegan Rd., North Chicago, IL 60064, USA.
E-mail: kedar.vaidya@abbvie.com

Received 4 January 2017; Revised 23 May 2017; Accepted 5 June 2017



1476-5586
http://dx.doi.org/10.1016/j.neo.2017.06.004

an average 5 year survival rate of 18%, the disease still represents an unmet medical need necessitating the search for additional therapeutic means. Expanding treatment options by generating new pharmaceuticals is one obvious avenue to attain this goal. To this intent, novel molecular drivers of the disease and preclinical models that mimic the physiological role of these molecules will have to be identified.

The traditional preclinical discovery cascade of cancer drugs has recently come under enhanced scrutiny. Specifically, the value of preclinical assays in predicting clinical efficacy has been questioned [3]. The heavy reliance on response of established cancer cell lines to cancer drugs in early stages of discovery was identified as a potential reason for failure of therapeutic responses in Phase II clinical trials [4]. These cell lines, grown in suspension or as monolayers on plastic, may be oversimplified models that are unlikely to recapitulate the pathology of the cancer type that they represent [4]. To enhance the relevance of the cancer models used in early discovery, the use of three-dimensional cell aggregates has received renewed attention as alternative or supplemental models for early drug screening. Three-dimensional (3D) cultures of tumor cells have been implemented in cancer research for at least half a century (for review see [5]). These models have a tumor-like configuration [5] and may help elucidate properties of experimental pharmaceuticals that are influenced by the histotypic cell configuration and consequently are impossible to study in monolayer or cell suspension. Examples of such properties are: penetration of drug through multiple cell layers [6] or the 'barrier effect' [7] encountered by therapeutic monoclonal antibodies. The use of 3D cultures yields also the practical advantage of assessing effects of prolonged drug exposures because 3D cultures can be perpetuated for several weeks while monolayer cultures usually last less than a week. Comparative studies between cells grown in 2D (monolayer) and 3D revealed the different expression of several genes in 3D cultures generating a transcriptional profile (TP) more similar to patient samples [8]. To identify cancer functions that are active in 3D rather than in 2D cultures, we generated the TP of NSCLC cells (NCI-H1650 and EBC-1) from both modes of culturing. TPs of the cultures *in vitro* were compared to one another and to the TP of matching xenografted tumors. Because confluence of monolayer cultures, size of the spheroids and volume of xenografted tumors possibly altered TPs, we compared intra- and inter-culture conditions using samples with defined confluence, size (diameter) or volume, respectively. A knowledge based tool, Ingenuity Pathway Analysis (IPA) was used to predict differences in pathway activation among tumor cells grown in various culture modes. The present study suggests that a limited number of signal transduction pathways active in NSCLC xenografts may be better represented by 3D than by 2D cultures *in vitro*. These pathways involved the following functions: hypoxia, angiogenesis, differentiation and inflammation. Whether parts of the TPs of xenografted tumors were mirrored by TPs of cultured cells *in vitro* not only depended on the 2D or 3D nature of the cultures but also on their confluence or diameter.

## Material and Methods

### *Cell Lines*

NCI-H1650 (adenocarcinoma of the lung; labeled H1650 hereafter) was obtained from the American Type Tissue Collection (ATCC, Manassas, VA). The cells were maintained in monolayer culture in RPMI1640 (Invitrogen, Carlsbad, CA) supplemented with 10% Fetal Bovine Serum (FBS, Hyclone, Logan, UT). Culture medium that contains all supplements is hereafter called complete culture medium. EBC-1 (squamous cell carcinoma of the lung) was obtained from the Japanese Collection of Research Bioresources Cell Bank (JCRB, Osaka, Japan). The cells were maintained in monolayer cultures with MEM medium (Invitrogen) supplemented with 10% FBS.

### *Monolayer (2D) Cultures*

Cells were seeded in 10 cm dishes at $10^5$ cells in 10 ml of cultured medium. The monolayer cultures were continued until confluence of 30, 60, 90 or 100% of the surface was reached. RNA was extracted at each of these confluence levels.

### *Spheroid (3D) Cultures*

*Generation of Spheroids.* Cells were plated at 1000 cells/100 µl medium in each well of 96-well round bottom plates (low attachment, Corning #7007). The plates were then centrifuged at 500 x g for 5 min. Plates were carefully moved to an incubator where aggregation was allowed for 72 h. For EBC-1 and H1650, this procedure usually generated spheroids with a diameter of approximately 0.2 mm.

*Growing of Spheroids.* Spheroids were further cultured in static conditions as originally described by Yuhas et al. [9]. Spheroids with a diameter of 0.2 mm were transferred to 24 multi-well plates that contain 0.5 ml agar underlay (0.66% agarose in complete RPMI culture medium) in each well. One spheroid was placed in each agar coated well and an overlay of 1 ml of culture medium was added. Spheroids were further cultured in an incubator (37 °C, 100% humidity, 5% $CO_2$ in air) and their growth was monitored by periodic measurement of their diameters by means of a calibrated graticule in the eyepiece of a stereoscope. During the observation period, medium was replaced twice a week. Samples with diameters (∅) of 0.2, 0.4, 0.8 or 1.2 mm were then selected for RNA extraction. Only samples with a round shape (perpendicular diameters differ less than 0.05 mm) were chosen.

*Processing of Spheroids for Histology.* The spheroids were placed in 10% neutral buffered formalin for 30 minutes. After fixation, spheroids were stained with 1% Alcian Blue (in 3% glacial acetic acid in water, pH 2.5) for 10 min and then washed repeatedly with phosphate buffered saline (PBS) to remove excess stain. After encasing the samples in 2% agarose, they were processed for paraffin embedding in a Sakura Tissue-Tek VIP processor (Nagano, Japan) for stepwise dehydration (45 min for each step) in 70%, 80%, 95% and finally 100% Ethanol. Subsequently the samples were immersed in xylene for 2 sessions of 45 min each and then embedded in paraffin thrice for 45 min each. Spheroids were cut in 4 µm serial sections, deparaffinized in xylene and rehydrated in a graded alcohol series and stained with hematoxylin and eosin prior to mounting of the sections on glass slides.

### *Generation of Xenografts*

Tumor cells suspended in culture medium were mixed 1:1 (v:v) in Matrigel. Five million cells in a total volume of 100 µl were injected subcutaneously in the right flank of female SCID/bg Mice (Charles River Laboratories, Wilmington, MA). H1650 and EBC-1 were both inoculated in 20 mice. Twice a week, perpendicular tumor diameters were measured by means of calipers and the tumor volume was calculated according to $V = L*W^2*0.5$. L stands for the larger of the 2

diameters and W for the shorter one. Tumor samples of 200, 400, 800, and 1000 $mm^3$ were collected and RNA was extracted. Messenger RNA was extracted from 3 tumors of each size category.

### *Animal Husbandry*

The mice were obtained from Charles River (Wilmington, MA). Ten mice were housed per cage. The body weight upon arrival was 18–20 g. Food and water were available *ad libitum*. Mice were acclimated to the animal facilities for a period of at least one week prior to commencement of experiments. Animals were tested in the light phase of a 12-hour light: 12-hour dark schedule (lights on at 06.00 hours). All experiments were conducted in compliance with AbbVie's Institutional Animal Care and Use Committee and the National Institutes of Health Guide for Care and Use of Laboratory Animals guidelines in a facility accredited by the Association for the Assessment and Accreditation of Laboratory Animal Care (AAALAC).

### *RNA Isolation and Gene Expression Microarray*

Monolayers, spheroids and tumor fragments were rinsed with PBS and frozen at −80 °C. Cells as well as tumor xenograft samples were lysed using Qiazol lysis reagent (Qiagen, Hilden, Germany) followed by RNA extraction with Qiagen RNeasy mini kit columns (Qiagen) according to manufacturer protocols. RNA purity and integrity were checked on Agilent Bioanalyzer 2100 (Agilent Technologies, Santa Clara, CA). RNA was subsequently used for gene expression Affymetrix microarray analysis (Thermo Fisher, Affymetrix, Santa Clara, CA). RNA was converted to biotin labeled cRNA using the 3′ IVT plus kit. The labeled cRNA was fragmented and loaded onto Human Genome U133 Plus 2.0 Arrays. Washing, staining and scanning of Affymetrix arrays used Affymetrix equipment. All procedures were according to manufacturer protocols.

### *Gene Expression Analysis, Statistics, and Bioinformatics*

Rosetta Resolver gene expression data analysis system (IBM) was used to normalize raw microarray data, calculate gene expression index and determine significant changes between different experimental conditions. The *P*-values were adjusted to control for False Discovery Rate (FDR) using q-value method [10]. Q-value ≤0.2 and fold change ≥2 or ≤ −2 were used as the statistical cut-offs to select differentially expressed genes. The selected differentially expressed genes were subjected to bioinformatics analysis using QIAGEN's Ingenuity Pathway Analysis (IPA,QIAGEN, Redwood City, CA, www.qiagen.com/ingenuity), where the significantly enriched canonical pathways, functions and upstream regulator effects were selected. The significance of a relatively activate or inactive pathway, function or regulatory effect, was measured by Z-score, where Z-scores ≥2 or ≤ −2 were the statistical cut-offs for significance. The upstream regulator analysis tool of IPA was used to predict alterations of transcriptional regulators associated with changes in culture conditions or progression. IPA defines upstream regulators as any molecule that can affect the expression of other molecules. [http://www.ingenuity.com/products/ipa].

### *QuantiGene Plex Assay for RNA Expression Assessment*

The QuantiGene Plex Assay was performed according to manufacturer's protocol (Thermo Fisher/Affymetrix, Santa Clara, CA). Briefly, RNA samples were incubated overnight with probe sets panel specific for genes of interest and housekeeping genes designed and manufactured by Affymetrix. The signal of target gene mRNA was amplified through branch DNA (bDNA) technology. The final signal was read by using a Luminex FlexMAP 3D instrument (Luminex, Austin, TX) and data was recorded as mean fluorescent intensity (MFI). The MFI of the genes of interest in each sample was normalized to MFI of housekeeping genes.

## Results

We compared the TPs of H1650 and EBC-1 when cultured in three conditions, namely: monolayer (2D) and spheroid cultures (3D) *in*

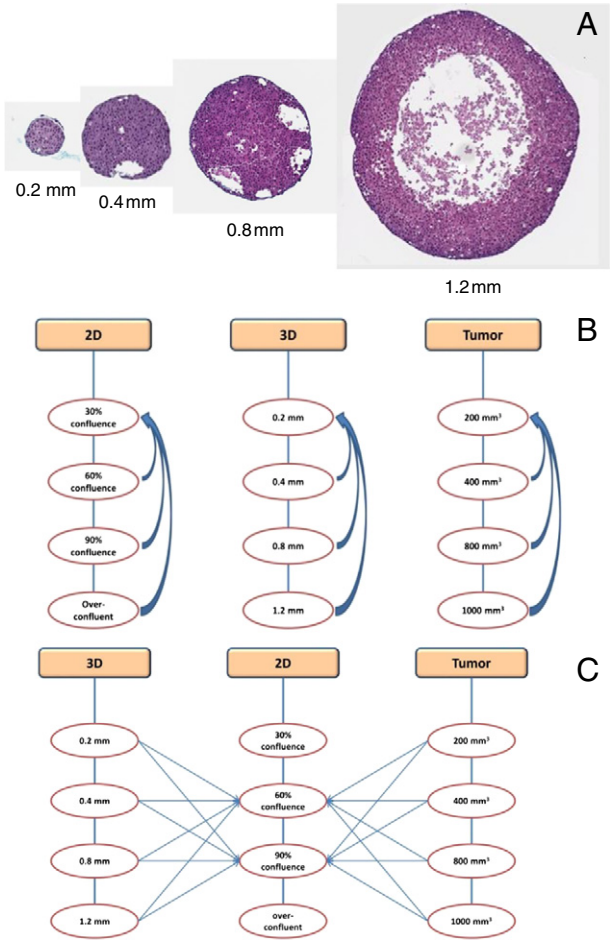


**Figure 1.** Study design to compare transcriptional profiles of NSCLC cells cultured *in vitro* and grown as xenografts. Transcriptional profiles of 2D monolayer (2D), 3D spheroid cultures (3D) as well as xenografted tumors (Tumor) of H1650 were generated. The histological organization of NSCLC 3D cultures (A) evolved from a morphologically homogeneous cell population (∅ = 0.2 and 0.4 mm) to a structure with 3 distinct cell layers (∅ = 0.8). From the periphery to the center a zone with proliferative cells, a zone with healthy cells in stasis and a core of necrotic cells with pyknotic nuclei are recognized. At ∅ = 1.2 mm the core of the culture consists out of necrotic material. Peripheral cavities are probably pseudo glandular structures and are seen at the four spheroid sizes. B is a schematic of the Intra-cultural comparisons of TPs: monolayers with higher confluence, larger spheroids or tumors are compared to the least confluent monolayer, or smallest sample, respectively. C describes the inter-cultural comparisons of TPs. To evaluate differences between cultures in 2D, 3D and as xenograft, TPs of each spheroid and xenograft condition were compared to the TP of 2D monolayer cultures at 60% and 90% confluence.

*vitro* as well as subcutaneous xenografts. Morphological changes and altered histological organization of the tumor cells are to be expected during the progression of these cultures. Figure 1*A* illustrates these changes in progressing spheroid cultures of H1650 in particular. As the spheroid grows a transition occurs from a tissue composed of morphologically homogeneous cells to a tissue organization that comprises 3 distinct areas, *i.e.* a core composed of necrotic material, a layer with pyknotic cells and a layer containing healthy and proliferating cells. To understand which cancer functions are likely represented in the various culture conditions and their state of progression, we made two types of comparisons of the TPs. On the one hand, the intra-cultural comparisons (Figure 1*B*) seek to address whether within each condition certain cancer functions are only represented by a specific cell density, spheroid size or tumor volume. On the other hand, the intercultural comparisons (Figure 1*C*) seek to identify the cancer functions that are uniquely active in a certain culture condition *in vitro* (2D or 3D) or in xenograft tumors regardless of the progression of the culture. For both intra- and intercultural comparisons, the analysis of TPs comprised global gene expression profiling, statistical analysis of differential expression and pathway and function analysis of transcriptional regulators.

### *Unsupervised Hierarchical Clustering*

The heat map shown in Figure 2 illustrates unsupervised hierarchical clustering of mRNA expression levels of H1650 and EBC-1 under the three different culturing conditions. The color-scale reflects the Z-score indicating each gene's deviation from the mean. TPs of EBC-1 and H1650 are distinct regardless of their culturing method. This finding may be a reflection of the different origin of the two cell lines. Nonetheless, within the transcriptional profile of each cell line, expression clustering is seen as a function of the culturing mode. Cells grown as xenografts have a distinct transcription profile

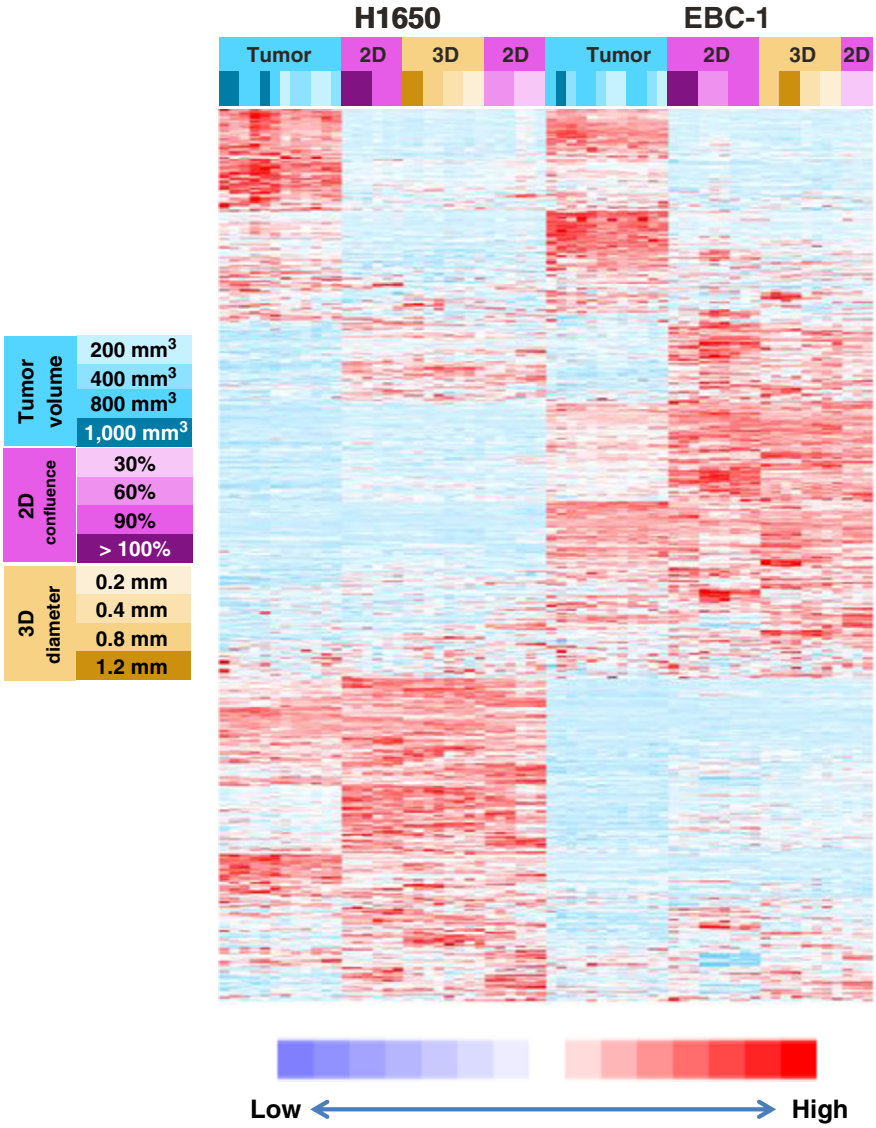


**Figure 2.** Transcriptional profiles of H1650 and EBC-1 cultured in 2D and 3D culture *in vitro* and as subcutaneous xenograft *in vivo*. The heat map reflects unsupervised hierarchical clustering of gene expression. The mRNA level of the genes relative to the mean gene expression is shown in the rows. The color scale (bottom of the figure) reflects the Z-score indicating each gene's deviation from the mean. The changes as a function of the culturing conditions are organized in the columns. The color code for the culturing conditions and their progression stage is depicted at the left of the heat map.

from cells grown in 2D and 3D cultures. Some of the distinct features in xenografts may be attributable to the interaction of tumor with host stromal cells. Because the hybridization probes in the microarray are designed to recognize human sequences, the distinct transcriptional profile of xenografts is unlikely a direct reflection of the mRNA content of the murine stromal cells. Differences in TPs between 2D and 3D cultures are not as conspicuous as the distinction between TPs of xenografts and cultures *in vitro*. Of note is that TPs of 3D cultures are clustered between sparse and dense monolayers. For further analysis, the mRNA of the biological repeats at each culture condition was combined. The validity of this approach was indicated by the reproducibility of the transcriptional profile of the biological replicates (Figure 2). The evaluation of the TPs of EBC-1 yielded similar conclusions as the TPs of H1650. The analysis of EBC-1 is presented in Supplementary Tables 1 and 2.

### *Identification of Intracultural Transcriptional Changes*

We determined changes of the gene expression profile of H1650 cells within each culturing modality (Figures 1*B* and 3, *A* and *B*). A change in gene expression of at least two-fold with a $P \leq .05$ was considered significant. For 2D cultures, the number of expression changes of monolayers grown to a confluence of 60, 90 or >100% were evaluated relative to monolayers with confluence of 30%. Similarly, the number expression changes of spheroids grown to 0.4, 0.8, and 1.2 mm diameter (∅) and of xenografts grown to 400, 800, and 1000 $mm^3$ were calculated relative to spheroids with ∅ = 0.2 mm and xenografts with a volume of 200 $mm^3$, respectively. The number of gene changes for each of the intra-cultural comparisons is indicated by the open arrow in Figure 3*A*. As illustrated in Figure 3*B*, increment of monolayer confluence, spheroid diameter or xenograft volume related directly to a larger number of gene expression changes.

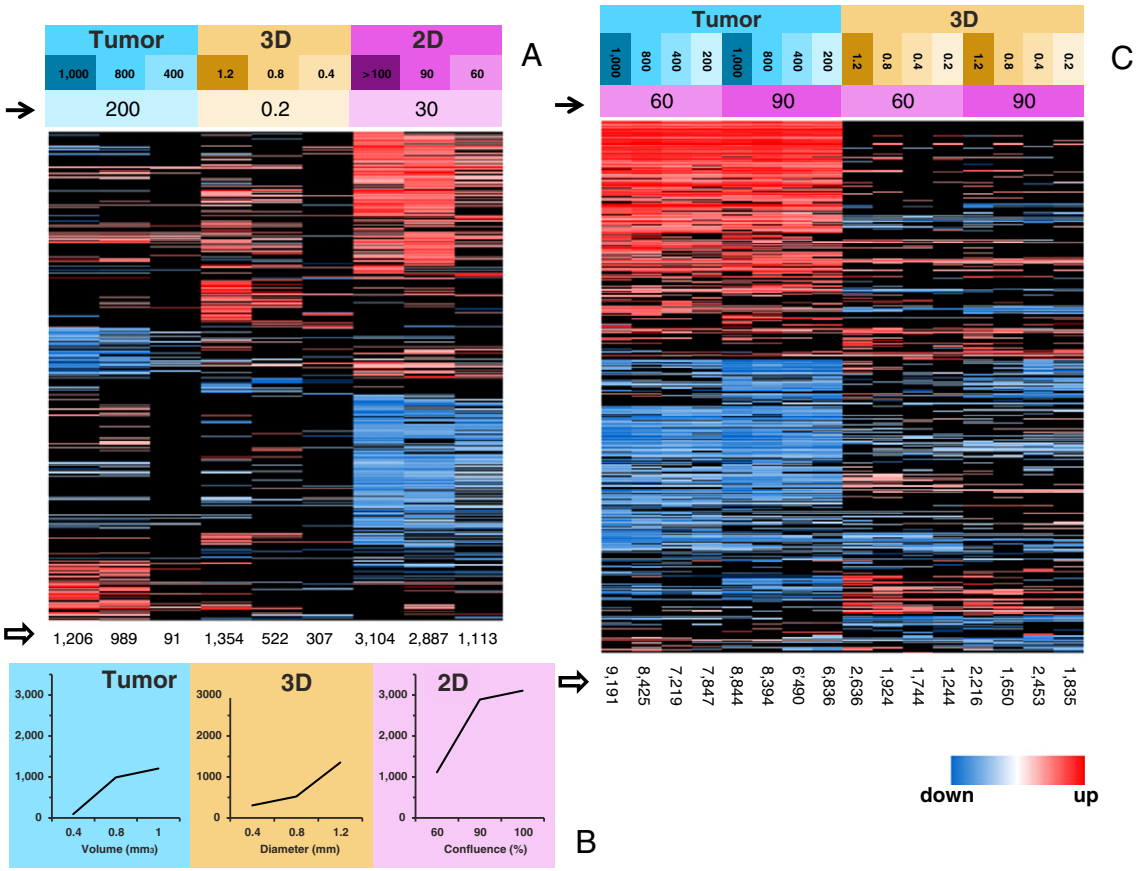


**Figure 3.** Changes in gene expression by progression of cultures (intracultural) and by altered culture conditions (intercultural). Panel A shows the mRNA expression level of H1650 cells grown as xenografts and as 3D and 2D cultures *in vitro*. The rows represent the various probe sets (genes) where only probes with ≥2 fold change and a $P \leq .05$ in at least one of the comparisons were plotted. Columns reflect the changes in expression levels of the progression stage within each culturing condition (tumor, 3D, and 2D) relative to their initial confluence or size (closed arrow). Progression stages for tumors are 1000, 800 and 400 $mm^3$ tumor volume. For 3D cultures, the stages are 1.2, 0.8, and 0.4 mm diameter. 2D cultures are staged at >100, 90, and 60% confluence. The open arrow indicates the number of significant gene changes of each condition and stage relative to their reference (closed arrow). Xenograft tumors, 3D spheroid cultures, and 2D monolayer cultures were compared to the smallest tumors (200 $mm^3$), spheroids (0.2 mm in diameter) or to sparse culture (30% confluence), respectively. The rows represent the genes (probesets) with significant difference in expression (≥2 fold change and a $P \leq .05$). The color scale (bottom of the figure) reflects the fold change in gene expression and black represent probes with $P > .05$ in a comparison. Panel B illustrates the number of gene changes (ordinate) for each stage of the 3 culture conditions (abscissa) as compared to the reference culture. Panel C shows the gene expression changes of H1650 cells induced by two culturing conditions (3D *in vitro* and xenograft *in vivo*) relative to 2D cultures. The columns reflect each of the culturing conditions and their stage of culture. The number of significant expression changes (indicated by open arrow) is calculated relative to 2D cultures at 60 or 90% confluence (closed arrow).

Significant expression changes with increased confluence in monolayer cultures were more numerous than changes in spheroids with increasing diameter and tumors with increasing volume. Specifically, the number of changes of smaller spheroids (*i.e.* ∅ = 0.2 mm *vs.* ∅ = 0.4 mm) and tumors (200 $mm^3$ *vs.* 400 $mm^3$) was more similar than the number of changes in subconfluent monolayer cultures (30% *vs.* 60%). These small spheroids and tumors differentially expressed 307 and 91 genes, respectively. In contrast, 1113 genes were differentially expressed between monolayers at a confluence of 30 and 60% (Figure 3*A*). However, the relative increment of expression changes during spheroid culture and xenograft growth was more pronounced than in monolayer cultures (Figure 3*B*). Progression of the latter cultures from 60% to over-confluence increases the number of expression changes relative to a 30% culture 2.8-fold (from 1113 to 3104). In comparison, progression of spheroid cultures from ∅ = 0.4 mm to ∅ = 1.2 mm increased the number of changes 4.4-fold (from 307 to 1354) relative to cultures with ∅ = 0.2 mm. In xenografts growing from 400 to 1000 $mm^3$ the number of expression alterations was 13.3-fold (from 91 to 1206) relative to tumors with a volume of 200 $mm^3$. These observations indicate that the dynamic of the magnitude in expression changes differ when cells are grown in 2D, 3D or as xenograft. Whereas the majority of changes in 2D cultures happen earlier during the culture, changes are more pronounced at later progression points in 3D cultures and xenografts.

### *Identification of Intercultural Expression Changes*

Alterations of the TPs of xenografts and spheroids as compared to monolayer cultures with a confluence of 60 and 90% were calculated (Figures 1*C* and 3*C*). Similar to the analysis of intra-cultural transcriptional changes, a twofold change at minimum along with a $P \leq .05$ was considered significant. The number of genes altered by growing the cells as spheroids or tumors was influenced by the confluence of the monolayer culture. For example, the number of significantly up-regulated and down-regulated genes in ∅ 0.4 mm spheroids as compared to 60% monolayer cultures was 656 and 1088, respectively. A comparison of the expression profile of these spheroids with the profile of a 90% confluent monolayer yielded 596 down-regulated and 1857 up-regulated genes. Cells in xenografts have a higher (min = 6490 and max = 9191) number of genes that are differentially expressed from monolayers as cells grown as spheroids (min = 1244 and max = 2636). This quantitative difference indicates that the growing cells in 3D did not necessarily induce a phenotype similar to cells grown as xenografts. To further understand the potentially unique phenotypes represented by 3D cultures, we used Ingenuity Pathway Analysis (IPA) to answer two questions. First, we evaluated whether certain cancer functions are uniquely represented by a specific 2D monolayer cell density, by 3D spheroid diameter or by xenografted tumor size. Second, the analysis aimed to discern whether certain cancer functions were reflected by 3D cultures *in vitro* and xenografts but were absent in 2D cultures.

### *Are Certain Cancer Functions Only Represented by a Specific 2D Culture Cell Density, 3D Spheroid Diameter or Tumor Size?*

The number of alterations in gene expression levels of the various culture conditions and modalities reveal that the transcriptional profile of H1650 cells not only varies in function of the mode of culture but also during the evolution of culturing the cells within a given culture modality. IPA revealed several potential signaling pathways associated with the progression of cell culture. This analytical algorithm identifies a set of relevant networks from a list of genes. IPA uses the records maintained in the ingenuity pathway knowledge base [11,12]. A calculated 'activation Z-score [13]' ≥ 2 reflects the significance of changes in expression of networks for a given comparison of culturing methods.

As shown in Figure 4*A*, hypoxia inducible transcriptional networks regulated by HIF1α, EPAS1 (encodes for HIF2α) and ARNT2 are predicted to be activated with increasing size of spheroids and tumors. Significant activation of HIF1α and EPAS1 was predicted when TPs of spheroids with a diameter of 0.8 or 1.2 mm were compared to spheroids with diameter of 0.2 mm and in large tumors (800$mm^3$ and 1000$mm^3$) compared to small tumors (200 $mm^3$). Transcriptional networks regulated by ARNT2 were only activated in spheroids with diameter of 1.2 mm. Details of the expression patters of HIF1α downstream genes under various culture conditions are depicted in Figure 4*B*. Of note, the induction of hypoxia related transcription happens exclusively during the culturing of tumor cells as spheroids and as xenografts. Increasing the confluence of the monolayers does not induce hypoxia related transcriptional regulators.

Examples of other cancer functions (Table 1) affected by the progression of H1650 tumor cells *in vitro* and *in vivo* as identified by IPA were associated with proliferation, angiogenesis, cell migration and fatty acid synthesis. TPs associated with cell cycle progression and mitosis become down-regulated as the 2D cultures progress. These functions were unaffected by progression of the 3D cultures and xenografts (Table 1A). Indeed, marked decreases in the expression of genes associated with these biological functions (*CDC25A*, *FOXM1*, *CCNA2*, *CHEK1* and *AURKB*) were confirmed to be down regulated with increased confluency of the culture (Supplementary fig. 1). Upstream regulators that influence functions such as *e.g.* MYC, Rb and E2F, are listed in Table 1B. While functions related to proliferation and cell viability were inhibited during the progression of monolayer cultures, activation was observed in 3D cultures and xenografts with increment of their volume. TPs, related to cell movement and migration, predict inhibition of these functions as 2D cultures progress. In contrast, up-regulation was predicted for progressing 3D cultures and xenografts. Functions associated with angiogenesis followed a similar trend. Genes modulated in these functions include ANG, APOE, CA9, CCR2, COL4A2, CTGF, IL8, EGFR, FGFR1, FN1, ICAM1, LOX, MST1, TGFA, TGFB2, TIMP2, TIMP3, and VIM (Supplementary fig. 2). Fatty acid metabolism, a major function necessary for energy provision to tumor cells [14], is also affected by the progression of cultures. In 2D cultures, up-regulation is only predicted at 60% confluence but not at 90 and >100%. Up-regulation of these functions is seen for larger spheroids and xenografts. In addition, IPA predicts major changes during the progression of cultures of several interleukin pathways (Table 1B). With the exception of IL6RN and IL27, these upstream regulators are mainly unaltered or inhibited during progression of 2D cultures but activated during progression of both 3D cultures and xenografts. The latter finding is consistent with increased proliferation and viability.

### *Are Certain Cancer Functions Reflected by 3D Cultures In Vitro and Xenografts but Absent in Monolayer Cultures?*

We identified the signaling pathways that were significantly altered in by culturing H1650 as 3D cultures *in vitro*. As shown in Figure 3*C*, the number of genes altered in 3D cultures as compared to

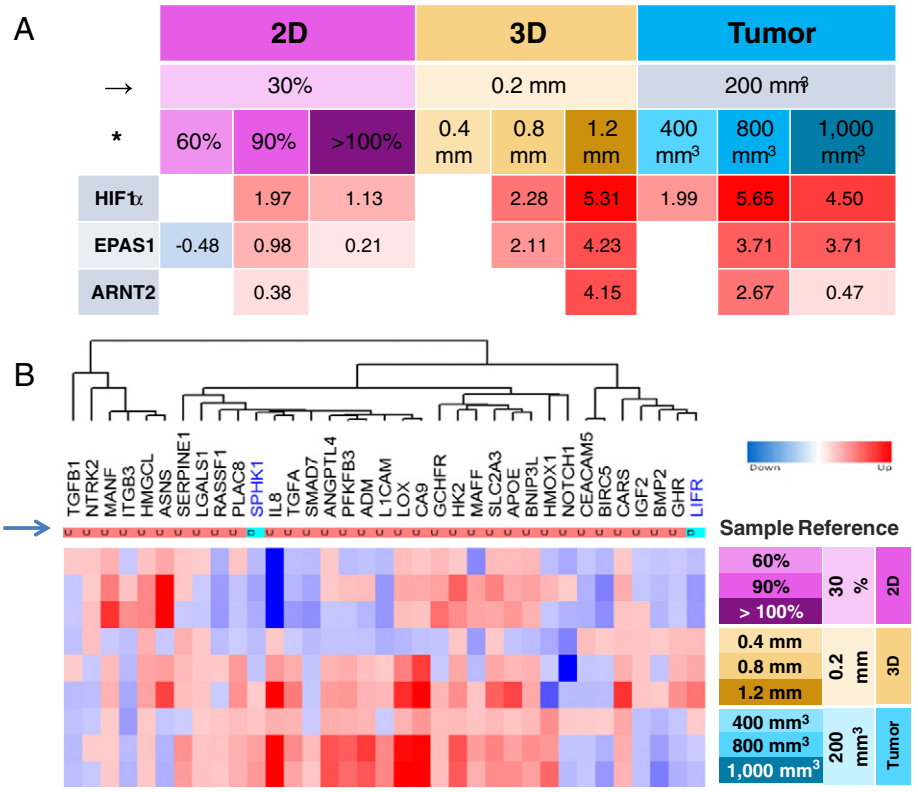


**Figure 4.** Alterations of hypoxia related transcription regulators in H1650 cells during progression of different culture modalities *in vitro* and *in vivo*. Panel A shows the activation Z-scores for hypoxia-related transcription factors HIF1α, EPAS1 and ARNT2. IPA Upstream Regulator analysis predicts activation of hypoxia-related transcription factors in large spheroids and tumors. Activation Z-scores are presented for intra-cultural comparisons of progressed cultures (asterisk) to their initial cultures (arrow). Z-scores ≥2 are considered significant. Panel B is a detailed heatmap of up(red)- and down(blue)-regulated HIF1α target genes. The blue arrow indicates the direction (U = up, D = down) of individual gene expression changes consistent with activation of HIF1α according to Ingenuity Knowledge Base. Columns of the heatmap reflect the direction of the individual gene expression change of progressed cultures (rows) compared to their reference culture.

monolayers varies with the diameter of the spheroids at the time of sampling. This number increases as a function of the diameter augmentation. The trend is clearly observed for the comparison of spheroids with 60% confluent monolayers but is disappearing when comparisons are made with 90% confluent monolayers. IPA predicted activation of hypoxia related transcription regulators (HIF1α, EPAS1, ARNT and ARNT2) for spheroids with ∅ >0.8 mm relative to monolayers with confluence of 60% (Figure 5). Increase in only HIF1α and EPAS1 is predicted for spheroids ≥1.2 mm relative to monolayers with confluence of 90%. The activation of hypoxia related transcriptions regulators in larger spheroids is consistent with activation in larger tumors when both were compared to 60% confluent monolayers. When compared to 90% confluent monolayers the activation is only seen in larger spheroids. Genes modulated downstream of HIF-1α include *TGFA, ADM, CA9, ANGPTL4, APOE, LOX, IL8*, and *L1CAM* (Supplementary Figure 3).

IPA of intra-cultural comparisons showed several examples of functions that were significantly and consistently up-regulated during progression of 3D cultures and xenografts and not in 2D cultures. As shown Table 2A, transcriptional networks associated with cellular movement and migration functions were enriched in tumors compared to monolayers. This enrichment was not observed when 3D cultures were compared to monolayers. Transcriptional networks associated with interferon as upstream regulator were activated when 3D cultures were compared to monolayers (Table 2B). However, by comparison of xenografts to monolayers an inhibition of these upstream regulators was demonstrated. Comparing TPs of tumors or 3D cultures to monolayers showed respectively an up- or down-regulation of transcriptional networks associated with MAP-kinase signaling. TPs associated with TGF and Wnt-catenin signaling as well as regulation of Epithelial Mesenchymal Transition were up-regulated in 3D cultures and xenografts when compared to monolayers.

## Discussion

The presented analysis of TPs of cancer cells cultured as monolayers or spheroids *in vitro* and grown as subcutaneous xenografts demonstrated that these profiles were subject to changes as a function of culture progression. A limited number of cancer functions were uniquely attributable to the culturing in 3D. These findings are relevant within the context of the rediscovered value of 3D cultures of cancer cells *in vitro* as a supplementary tool to screen for efficacious new cancer therapeutics.

The attrition rate of new cancer drugs in the clinic is as high as 98%. The lack of efficacy of these compounds is viewed as the major reason for clinical failure [15,16]. Furthermore, the poor predictability of preclinical models has been accentuated as a prominent culprit

Table 1. Examples of disease & functions (A) and upstream regulators (B) predicted By IPA to alter during progression of NSCLC H1650 (intra-cultural comparisons) in 2D and 3D cultures *in vitro* or as xenografted tumors *in vivo*

**A**

| | 2D (%) | | | 3D (mm) | | | Tumor (mm3) | | |
|---|---|---|---|---|---|---|---|---|---|
| → | 30 | | | 0.2 | | | 200 | | |
| * | 60 | 90 | >100 | 0.4 | 0.8 | 1.2 | 400 | 800 | 1,000 |
| **IPA Disease & Function** | | | | | | | | | |
| mitosis | | | -2.63 | | | | | | |
| cell cycle progression | -1.14 | -0.55 | -2.59 | | | | | | |
| proliferation of lung cancer cell lines | | -0.62 | -2.37 | | | -0.57 | | | |
| M phase | | -2.24 | -2.36 | | | | | | |
| S phase | | | -2.30 | | -0.87 | | | | |
| cell cycle progression of tumor cell lines | -0.71 | | -2.29 | | | | | | |
| S phase of tumor cell lines | | | -2.12 | | | | | | |
| mitosis of tumor cell lines | | | -2.06 | | | | | | |
| cytokinesis | | | -2.04 | | | | | | |
| proliferation of tumor cell lines | | -0.78 | -3.83 | 0.37 | | 2.16 | | 2.31 | -0.15 |
| cell viability | -0.65 | 0.20 | -2.31 | | 0.51 | 4.92 | | 3.20 | 1.66 |
| cell viability of tumor cell lines | | -0.38 | -2.51 | | | 4.10 | | 2.17 | 2.06 |
| proliferation of cells | -0.07 | -0.10 | -2.20 | | 1.07 | 3.59 | | 2.94 | 0.18 |
| proliferation of epithelial cells | | | -1.50 | | | 2.14 | | | -0.57 |
| growth of epithelial tissue | 1.34 | -0.16 | 0.04 | -0.22 | 0.02 | 2.20 | | 1.38 | 0.69 |
| synthesis of DNA | | | -2.28 | | | 3.14 | | 2.89 | 1.91 |
| invasion of tumor cell lines | -0.34 | -1.49 | -2.31 | -0.78 | 0.13 | 2.34 | 0.99 | 3.21 | 2.11 |
| invasion of cells | -0.35 | -1.10 | -2.17 | -0.74 | 0.35 | 2.36 | 0.81 | 2.97 | 1.91 |
| migration of tumor cell lines | -1.31 | -0.46 | -2.03 | | -0.10 | 2.87 | 1.58 | 2.89 | 1.78 |
| cell movement | -0.41 | 0.87 | -1.26 | -1.13 | 0.58 | 3.44 | 0.82 | 3.17 | 1.08 |
| migration of cells | -0.19 | 0.86 | -1.40 | -1.40 | 0.49 | 3.32 | | 3.10 | 1.14 |
| cell movement of tumor cell lines | -1.38 | -0.57 | -1.95 | 0.00 | -0.12 | 2.83 | 0.88 | 3.00 | 1.97 |
| angiogenesis | 0.11 | 0.66 | 0.38 | | -0.39 | 2.86 | | 2.57 | 2.50 |
| tubulation of endothelial cells | -0.61 | | | | 0.73 | 2.75 | | | |
| movement of vascular endothelial cells | -0.21 | | | | -0.53 | 2.72 | | | 1.39 |
| tubulation of vascular endothelial cells | | | | | | 2.22 | | | |
| migration of endothelial cells | 0.56 | 1.17 | -1.05 | -1.00 | -0.66 | 2.21 | 1.00 | 1.77 | 1.55 |
| synthesis of fatty acid | 1.31 | | | | 0.87 | 2.23 | | | 0.03 |
| fatty acid metabolism | 2.08 | | | | | 2.15 | | 1.73 | 0.54 |
| metabolism of membrane lipid derivative | 0.49 | | | | | 2.13 | | | |

**B**

| | 2D (%) | | | 3D (mm) | | | Tumor (mm3) | | |
|---|---|---|---|---|---|---|---|---|---|
| → | 30 | | | 0.2 | | | 200 | | |
| * | 60 | 90 | >100 | 0.4 | 0.8 | 1.2 | 400 | 800 | 1,000 |
| **IPA Upstream *Regulator*** | | | | | | | | | |
| MYC | -1.63 | -1.98 | -3.16 | | -2.02 | -0.62 | | 0.31 | -0.58 |
| FOXM1 | | -2.14 | -2.97 | | | | | | |
| E2f | | -3.10 | -2.81 | | | | | | |
| RBL1 | | 1.91 | 2.16 | | | | | | |
| CDKN2A | -0.86 | 0.85 | 2.29 | | 1.66 | | | | 0.36 |
| RBL2 | | | 3.20 | | | | | | |
| IL17A | 0.30 | 1.80 | | | -0.55 | 2.58 | | 2.66 | 2.86 |
| IL1A | -0.39 | 0.23 | 0.10 | -1.98 | | 2.65 | | 2.74 | 2.94 |
| IL1B | -0.68 | -0.92 | -0.31 | -0.26 | -0.52 | 3.38 | -0.45 | 3.12 | 2.28 |
| IL2 | 0.83 | 2.30 | | | 0.91 | 2.56 | | 1.65 | 1.20 |
| IL6 | 0.40 | 1.22 | 1.14 | | 1.22 | 2.12 | -0.80 | 2.36 | 1.58 |
| IL6R | 0.90 | | | | | 2.80 | | 1.98 | 2.18 |
| IL6RN | | -0.29 | -2.31 | -2.00 | | -3.33 | | -0.67 | 0.45 |
| IL27 | 0.23 | 2.64 | 2.66 | 1.74 | 0.64 | | | -2.62 | -2.04 |

The number in the table represents an activation Z-score. The arrow indicates the reference culture for comparison to the culture conditions indicated by *.

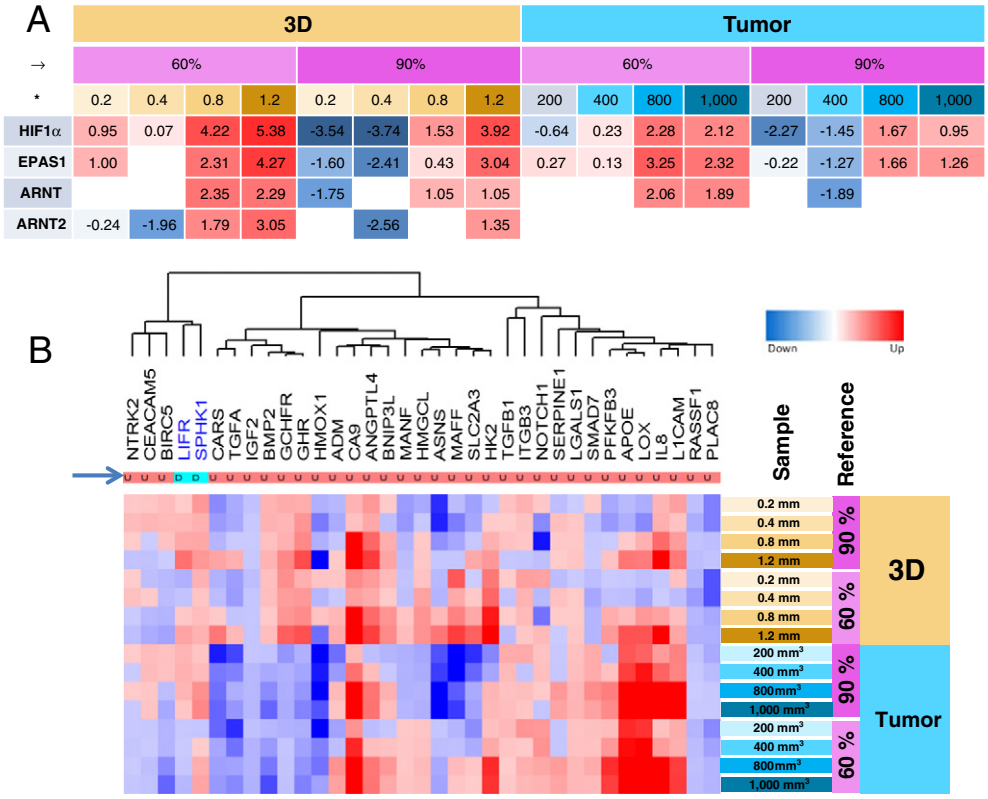


**Figure 5.** Alterations of hypoxia related transcription regulators in H1650 cells depending on the mode of culturing. Panel A shows the activation Z-scores for hypoxia-related transcription factors HIF1α, EPAS1, ARNT and ARNT2. IPA Upstream Regulator analysis predicts activation of hypoxia-related transcription factors in large spheroids and tumors. Activation Z-scores are presented for inter-cultural comparisons of progressed cultures (asterisk) to 2D cultures with confluence of 60% and 90% (arrow). Z-score ≥ 2 are considered significant. Panel B is a detailed heatmap of up(red)- and down(blue)-regulated HIF1α target genes. The blue arrow indicates the direction (U = up, D = down) of individual gene expression changes consistent with activation of HIF1α according to Ingenuity Knowledge Base. Columns of the heatmap reflect the direction of the individual gene expression change of progressed cultures (rows) compared to the reference cultures.

for the inefficiency of the drug development cascade [17,18]. One major purpose of preclinical models is to indicate the translatability of a drug's efficacy towards the clinic [17]. A failure in design or interpretation of these models can thus create the erroneous anticipation of beneficial activity of a drug in the clinic. Although there is no shortage of preclinical oncology models *in vitro* and *in vivo* (for review see: [19–23]) none of them are capable of replicating all aspects of cancer [24]. In view of the numerous types of cancer and the range of disease progression from a few months (*e.g.* pancreatic cancer, [25]) to several decades (*e.g.* colorectal cancer, [26]), it is inconceivable that any preclinical model could mimic the disease in its entirety. This improbability is further compounded by the evolution of cancer lesions during progression [27] that can induce variability of the cellular composition of lesions within the same patient at the time of treatment. In addition, selection pressure exerted by treatment can select for a relapsing tumor that remains irresponsive to original treatment. Improvement of the predictive capability of the preclinical model is therefore rather to be found in the understanding of which aspect of cancer progression the model represents than in an attempt to create an accelerated cancer progression in experimental conditions.

The regained interest in 3D models is fueled by the notion that these models can recapitulate the tissue architecture of the tumor [4,23]. Because the tissue structure in which the tumor cell resides can influence the cell's reaction to chemotherapy, the 3D models are viewed as more indicative than 2D monolayer cultures of a physiological response of tumor cells to chemotherapy. Indeed, the microenvironment can influence *e.g.* apoptosis [28], proliferation [29] and differentiation [30] of tumor cells. Although monolayer cultures have been a reliable staple of phenotypic screening in the cancer drug discovery for practical reasons, current technological advances [8,31] have made it possible to use 3D cultures in sufficiently high throughput to function as a replacement or supplemental phenotypic screen. Nonetheless, there still remains a major gap in the knowledge on how efficacy in these models translates to efficacy in a clinical setting.

We demonstrated the variability of TPs in specific modes of culture using models representing two distinct indications, NCI-H1650 (adenocarcinoma of the lung) and EBC-1 (squamous carcinoma of the lung). The analysis was not designed to unravel the accuracy of clinical translatability of one model over another but rather to understand how the preclinical models may evoke different properties of the same cancer cell. Our findings indicate that TPs and projected pathway activation or deactivation (as defined by IPA analysis reflecting up- or down-regulation of bio-functions and upstream regulators) of cancer cells depends not only on the mode of culturing but also on the progression of the culture. We found a limited number of genes that were significantly altered by growing tumor cell

Table 2. Examples of disease functions (A) and upstream regulators (B) predicted By IPA to alter in H1650 3D cultures and tumor xenografts (inter-cultural comparisons) as compared to 2D cultures at 60 and 90% confluence

**A**

| | 3D | | | | | | | | Tumor | | | | | | | |
|---|---|---|---|---|---|---|---|---|---|---|---|---|---|---|---|---|
| → | 60% | | | | 90% | | | | 60% | | | | 90% | | | |
| * | 0.2 | 0.4 | 0.8 | 1.2 | 0.2 | 0.4 | 0.8 | 1.2 | 200 | 400 | 800 | $10^3$ | 200 | 400 | 800 | $10^3$ |
| migration of cancer cells | −1.26 | | −1.10 | | | | | | 1.18 | 2.01 | 2.06 | 1.20 | 1.15 | | 2.23 | 1.69 |
| migration of tumor cells | | | −1.13 | | | −0.69 | −1.16 | 0.03 | 1.53 | 2.33 | 2.36 | 1.52 | 1.61 | 1.93 | 2.30 | 2.08 |
| movement of tumor cells | −1.16 | | −0.82 | | | −0.37 | −0.76 | 0.46 | 1.47 | 2.19 | 2.23 | 1.34 | 1.05 | 1.67 | 2.29 | 1.85 |
| movement of cancer cells | −1.36 | −0.91 | −1.00 | | −0.41 | −0.53 | | 0.58 | 1.38 | 2.07 | 2.03 | 1.63 | 1.47 | 2.06 | 2.35 | 2.15 |
| cell movement of carcinoma cell lines | | −2.09 | | 0.10 | | | −1.31 | −0.31 | | 2.84 | 4.21 | 3.55 | | | 3.65 | |
| invasion of cells | 0.04 | −0.17 | 0.45 | 1.19 | −1.30 | −2.62 | −0.61 | 0.37 | 1.23 | 2.35 | 3.74 | 2.62 | 0.33 | 1.68 | 2.80 | 2.29 |
| invasion of tumor cell lines | −0.26 | −0.30 | 0.42 | 1.18 | −1.14 | −2.19 | −1.05 | 0.48 | 1.33 | 2.66 | 4.06 | 2.59 | 0.88 | 1.77 | 3.19 | 2.49 |

**B**

| | 3D | | | | | | | | Tumor | | | | | | | |
|---|---|---|---|---|---|---|---|---|---|---|---|---|---|---|---|---|
| → | 60% | | | | 90% | | | | 60% | | | | 90% | | | |
| * | 0.2 | 0.4 | 0.8 | 1.2 | 0.2 | 0.4 | 0.8 | 1.2 | 200 | 400 | 800 | $10^3$ | 200 | 400 | 800 | $10^3$ |
| IFNB1 | −0.19 | 2.69 | 0.68 | 1.75 | 0.84 | 2.49 | 0.94 | 1.87 | −3.38 | −2.32 | −2.02 | −2.66 | −2.38 | −2.69 | −2.50 | −2.24 |
| IFNE | | | | | | 1.07 | | 1.98 | −2.43 | −1.98 | | −1.71 | | −2.43 | | |
| IFNA2 | | 3.93 | 2.96 | 4.72 | 0.34 | 4.21 | 2.87 | 5.45 | −2.43 | −2.57 | −2.58 | −3.94 | | −3.17 | −3.58 | −3.78 |
| IFNG | 2.26 | 4.60 | 3.90 | 5.10 | −2.34 | 2.03 | 0.38 | 3.46 | −2.25 | −1.33 | −0.54 | −2.15 | −5.22 | −3.59 | −3.46 | −3.76 |
| IFNK | | | | | | 1.00 | | | −2.24 | −2.00 | | −1.41 | | −2.24 | | |
| IFNL1 | | 3.05 | | 3.94 | 0.71 | 3.58 | 2.17 | 4.44 | −2.14 | −2.35 | −2.99 | −3.66 | | −2.50 | −2.21 | −2.54 |
| Ifn | 0.20 | 2.75 | 1.09 | 3.11 | 1.36 | 2.80 | 1.69 | 3.33 | −1.02 | −0.35 | −1.21 | −1.98 | −1.72 | −1.16 | −1.56 | −1.91 |
| ERK1/2 | −0.24 | −1.03 | 0.53 | 1.99 | −1.71 | −2.98 | −0.09 | 1.29 | 0.19 | 1.52 | 3.71 | 3.44 | 0.04 | 1.31 | 2.41 | 2.28 |
| P38 MAPK | −1.92 | −1.39 | −0.29 | 0.93 | −2.53 | −3.12 | −2.06 | −0.44 | 0.26 | 0.43 | 1.73 | 1.69 | −0.94 | 0.21 | 0.44 | 0.49 |
| AKT | 0.39 | −0.56 | 0.40 | 1.11 | −1.63 | −1.91 | −1.44 | −0.19 | 0.27 | 0.63 | 1.95 | 1.58 | 0.75 | −0.28 | 0.80 | 1.19 |
| ERK | 0.37 | −0.13 | 0.76 | 2.04 | −1.67 | −1.77 | −0.45 | 0.14 | 0.93 | 1.01 | 2.47 | 2.24 | 0.15 | 0.85 | 1.54 | 1.18 |
| jnk | −0.59 | −1.14 | −0.89 | −0.09 | −2.00 | −2.66 | −2.44 | −1.28 | 1.05 | 1.05 | 2.61 | 2.44 | −0.11 | 0.66 | 2.17 | 1.62 |
| TGF–Signaling | 1.19 | 2.94 | 2.48 | 2.59 | 2.85 | 3.57 | 1.86 | 1.54 | 3.02 | 2.84 | 2.23 | 2.68 | 2.85 | 2.55 | 2.37 | 3.13 |
| Wnt/catenin Signaling | 1.48 | 1.32 | 1.91 | 1.95 | 1.51 | 0.40 | 2.29 | 1.28 | 1.89 | 1.85 | 1.83 | 2.45 | 3.17 | 2.69 | 3.77 | 4.81 |
| Regulation of EMT | 3.53 | 1.66 | 2.29 | 1.67 | 2.84 | 0.86 | 3.93 | 1.56 | 3.11 | 2.87 | 3.39 | 3.04 | 2.36 | 2.94 | 5.19 | 6.93 |

Numbers in the table represent an activation Z-score. The arrow indicates the reference 2D cultures for comparison to the culture conditions indicated by *.

lines in 3D rather than in 2D cultures. Furthermore, the TPs of the 3D cultures bore a closer resemblance to those of 2D cultures than to the profiles of xenografted tumors. The differences observed in gene expression among the different modes and progression stages of cultures provides an indication of pathway evolution with time, as predicted by IPA. As shown in Supplementary Figures 1–3, transcription modulation observed by microarray of multiple genes involved in hypoxia, mitosis, cell cycle progression, angiogenesis, cell movement (migration, invasion) were determined. We confirmed that the trends in gene expression are reproducible and similar to the changes predicted by IPA analysis. The purpose of this study was not to define the biochemical activity of a specific pathway or individual pathway mediators, but to demonstrate that not all culture conditions are appropriate for determining targeted therapeutic agent response *in vitro* and *in vivo* due to changes in phenotypic characteristics and target expression. Based on our data, *a priori* knowledge rather than assumption of the impact of culture modalities (*in vitro* or *in vivo*) can be expected to better inform the investigator in the selection of models and better define testing conditions for biochemical assays. This type of transciptome comparison of various preclinical models has rarely been documented. Cody et al. [32] found that by comparing the TPs for chromosome 3 of ovarian cancer cells, the

mode of preclinical culturing only moderately influenced the transcriptome. The authors concluded therefore that using cultures of ovarian cancer lines was suitable to characterize expression of gene candidates underlying malignancy. Nonetheless, these findings are not inherently inconsistent with the idea that 3D cultures may have a higher likelihood of predicting effects of cancer therapeutics. Indeed, response to cancer drugs is not necessarily related to altered gene expression of the cancer cell. In this regard, the mimicry of a solid tumor's histological configuration by a 3D culture can alter the exposure of individual cells to chemotherapeutics. One major resistance mechanism to anticancer drugs is the limited distribution from blood vessels [33]. A 3D model can allow for the analysis and optimization of a drug's flux and consumption [33]. For antibody therapeutics, the 3D model allows for determining optimal affinity for maximal distribution (*e.g.* barrier effect, [7]).

As opposed to 2D cultures, phenotypic properties of 3D cultures such as cell to cell contact, formation of extracellular matrix, hypoxia and cell cycle heterogeneity can influence the efficacy of chemo- or radio-therapy [5,8,34]. Consequently, these properties can be expected to be reflected by different transcriptomes of 2D and 3D cultures. As our study suggests, one has to distinguish between differences in 2D and 3D that are caused by merely aggregating cells and differences that are a consequence of culture progression. While differences in transcriptional profiling between monolayers and smaller spheroids are negligible, predicted activation of pathways such as hypoxia, angiogenesis, inflammation and differentiation occurs when spheroids reach a diameter of approximately 0.8 mm. In other words, influence of the former pathways on performance of an experimental drug can only be expected when the 3D cultures reach a critical size.

Now that technical difficulties to generate and analyze 3D cultures are virtually eliminated these cultures can be used to aid drug development. In addition to the 3D cultures in static conditions, more complex systems are currently available. 3D models with cancer cells co-cultured with fibroblasts [35], cells cultured on a specific extracellular scaffold [36,37], cultures of integral tissue slices [38] as well as organoid cultures derived from primary tumors [39] are examples of models that attempt to present a cancer cell in a relevant tissue background. Although 3D models have shown altered responses to targeted therapies than cancer cells grown in monolayers (*e.g.* trastuzumab [40] and EGFR inhibitors [41]), the question of predictability of these models to the clinic still remains.

Development of cancer evolves over a period of months to several decades. During this time the cellular composition of a neoplastic tumor can drastically vary. Our results show that even the simplest of 3D models (static monocultures of established cancer cell lines) alter their phenotype during progression. Consequently, the specific pathophysiological aspects of the disease reflected by complex *in vitro* models may not only depend on the nature of the model but also on its progression over time.

In conclusion, differences in TPs of 2D and 3D cancer cell cultures are subject to progression of the cultures. The relevance of the model towards a cancer phenotype in the clinic is thus not necessarily given by the mode of culturing cancer cells. The presented data challenge the notion that a given model carries an inherent 'predictiveness' towards the clinical situation. At best the preclinical model may only reflect limited aspects of malignancy. The transcriptome of 3D cultures is consistent with the notion that these models are capable of mimicking aspects of cancer such as *e.g.* hypoxia, activation of angiogenesis, and differentiation signatures that are not reflected in 2D models. It should be emphasized that IPA analysis only reflects a probability score of alterations in certain signal transduction pathways. Nevertheless, the current study shows that successful implementation of 3D models will necessitate exhaustive phenotypic characterization to verify the relevance of implementing these models for drug development.

Supplementary data to this article can be found online at http://dx.doi.org/10.1016/j.neo.2017.06.004.

## Disclosure and Acknowledgements

ERB, XL, PEH, TPM, AO, MJM, KFD, JAH, TU, and KSV are Abbvie employees. VES and CB are affiliated with iBET. Work presented in the manuscript is part of a collaboration between Abbvie, iBET, and PREDECT. The research leading to these results has received support from the Innovative Medicines Initiatives Joint Undertaking under grant agreement number 11588, resources of which are composed of financial contribution from the European Union's Seventh Framework Programme (FP/2007–2013) and EFPIA companies' in kind contribution. VES and CB acknowledge iNOVA4Health - UID/Multi/04462/2013, a program financially supported by Fundação para a Ciência e Tecnologia/Ministério da Educação e Ciência, through national funds and co-funded by FEDER under the PT2020 Partnership Agreement.

## References

[1] Politi K and Herbst RS (2015). Lung cancer in the era of precision medicine. *Clin Cancer Res* **21**, 2213–2220.
[2] Siegel RL, Miller KD, and Jemal A (2016). Cancer statistics, 2016. *CA Cancer J Clin* **66**, 7–30.
[3] Wilding JL and Bodmer WF (2014). Cancer cell lines for drug discovery and development. *Cancer Res* **74**, 2377–2384.
[4] Hickman JA, Graeser R, de Hoogt R, Vidic S, Brito C, Gutekunst M, van der Kuip H, and Consortium IP (2014). Three-dimensional models of cancer for pharmacology and cancer cell biology: capturing tumor complexity in vitro/ex vivo. *Biotechnol J* **9**, 1115–1128.
[5] Mueller-Klieser W (1997). Three-dimensional cell cultures: from molecular mechanisms to clinical applications. *Am J Phys* **273**, C1109–C1123.
[6] Ackerman ME, Pawlowski D, and Wittrup KD (2008). Effect of antigen turnover rate and expression level on antibody penetration into tumor spheroids. *Mol Cancer Ther* **7**, 2233–2240.
[7] Graff CP and Wittrup KD (2003). Theoretical analysis of antibody targeting of tumor spheroids: importance of dosage for penetration, and affinity for retention. *Cancer Res* **63**, 1288–1296.
[8] Hirschhaeuser F, Menne H, Dittfeld C, West J, Mueller-Klieser W, and Kunz-Schughart LA (2010). Multicellular tumor spheroids: an underestimated tool is catching up again. *J Biotechnol* **148**, 3–15.
[9] Yuhas JM, Li AP, Martinez AO, and Ladman AJ (1977). A simplified method for production and growth of multicellular tumor spheroids. *Cancer Res* **37**, 3639–3643.
[10] Storey JD and Tibshirani R (2003). Statistical significance for genomewide studies. *Proc Natl Acad Sci U S A* **100**, 9440–9445.
[11] Ficenec D, Osborne M, Pradines J, Richards D, Felciano R, Cho RJ, Chen RO, Liefeld T, Owen J, and Ruttenberg A, et al (2003). Computational knowledge integration in biopharmaceutical research. *Brief Bioinform* **4**, 260–278.
[12] Calvano SE, Xiao W, Richards DR, Felciano RM, Baker HV, Cho RJ, Chen RO, Brownstein BH, Cobb JP, and Tschoeke SK, et al (2005). A network-based analysis of systemic inflammation in humans. *Nature* **437**, 1032–1037.
[13] Kramer A, Green J, Pollard Jr J, and Tugendreich S (2014). Causal analysis approaches in Ingenuity Pathway Analysis. *Bioinformatics* **30**, 523–530.
[14] Currie E, Schulze A, Zechner R, Walther TC, and Farese Jr RV (2013). Cellular fatty acid metabolism and cancer. *Cell Metab* **18**, 153–161.
[15] Maxmen A (2011). Translational research: The American way. *Nature* **478**, S16–S18.

[16] Hay M, Thomas DW, Craighead JL, Economides C, and Rosenthal J (2014). Clinical development success rates for investigational drugs. *Nat Biotechnol* **32**, 40–51.
[17] Mak IW, Evaniew N, and Ghert M (2014). Lost in translation: animal models and clinical trials in cancer treatment. *Am J Transl Res* **6**, 114–118.
[18] Kamb A (2005). What's wrong with our cancer models? *Nat Rev Drug Discov* **4**, 161–165.
[19] Hoelder S, Clarke PA, and Workman P (2012). Discovery of small molecule cancer drugs: successes, challenges and opportunities. *Mol Oncol* **6**, 155–176.
[20] Talmadge JE, Singh RK, Fidler IJ, and Raz A (2007). Murine models to evaluate novel and conventional therapeutic strategies for cancer. *Am J Pathol* **170**, 793–804.
[21] Toniatti C, Jones P, Graham H, Pagliara B, and Draetta G (2014). Oncology drug discovery: planning a turnaround. *Cancer Discov* **4**, 397–404.
[22] Workman P, Aboagye EO, Balkwill F, Balmain A, Bruder G, Chaplin DJ, Double JA, Everitt J, Farningham DA, and Glennie MJ, et al (2010). Guidelines for the welfare and use of animals in cancer research. *Br J Cancer* **102**, 1555–1577.
[23] Kimlin LC, Casagrande G, and Virador VM (2013). In vitro three-dimensional (3D) models in cancer research: an update. *Mol Carcinog* **52**, 167–182.
[24] Stock K, Estrada MF, Vidic S, Gjerde K, Rudisch A, Santo VE, Barbier M, Blom S, Arundkar SC, and Selvam I, et al (2016). Capturing tumor complexity in vitro: Comparative analysis of 2D and 3D tumor models for drug discovery. *Sci Rep* **6**, 28951.
[25] Zijlstra M, Bernards N, de Hingh IH, van de Wouw AJ, Goey SH, Jacobs EM, Lemmens VE, and Creemers GJ (2016). Does long-term survival exist in pancreatic adenocarcinoma? *Acta Oncol* **55**, 259–264.
[26] Zauber AG, Winawer SJ, O'Brien MJ, Lansdorp-Vogelaar I, van Ballegooijen M, Hankey BF, Shi W, Bond JH, Schapiro M, and Panish JF, et al (2012). Colonoscopic polypectomy and long-term prevention of colorectal-cancer deaths. *N Engl J Med* **366**, 687–696.
[27] Greaves M and Maley CC (2012). Clonal evolution in cancer. *Nature* **481**, 306–313.
[28] Zahir N and Weaver VM (2004). Death in the third dimension: apoptosis regulation and tissue architecture. *Curr Opin Genet Dev* **14**, 71–80.
[29] Quail DF and Joyce JA (2013). Microenvironmental regulation of tumor progression and metastasis. *Nat Med* **19**, 1423–1437.
[30] Bissell MJ, Radisky DC, Rizki A, Weaver VM, and Petersen OW (2002). The organizing principle: microenvironmental influences in the normal and malignant breast. *Differentiation* **70**, 537–546.
[31] Santo VE, Estrada MF, Rebelo SP, Abreu S, Silva I, Pinto C, Veloso SC, Serra AT, Boghaert E, and Alves PM, et al (2016). Adaptable stirred-tank culture strategies for large scale production of multicellular spheroid-based tumor cell models. *J Biotechnol* **221**, 118–129.
[32] Cody NA, Zietarska M, Filali-Mouhim A, Provencher DM, Mes-Masson AM, and Tonin PN (2008). Influence of monolayer, spheroid, and tumor growth conditions on chromosome 3 gene expression in tumorigenic epithelial ovarian cancer cell lines. *BMC Med Genet* **1**, 34.
[33] Minchinton AI and Tannock IF (2006). Drug penetration in solid tumours. *Nat Rev Cancer* **6**, 583–592.
[34] Sutherland RM (1988). Cell and environment interactions in tumor microregions: the multicell spheroid model. *Science* **240**, 177–184.
[35] Estrada MF, Rebelo SP, Davies EJ, Pinto MT, Pereira H, Santo VE, Smalley MJ, Barry ST, Gualda EJ, and Alves PM, et al (2016). Modelling the tumour microenvironment in long-term microencapsulated 3D co-cultures recapitulates phenotypic features of disease progression. *Biomaterials* **78**, 50–61.
[36] Fong EL, Lamhamedi-Cherradi SE, Burdett E, Ramamoorthy V, Lazar AJ, Kasper FK, Farach-Carson MC, Vishwamitra D, Demicco EG, and Menegaz BA, et al (2013). Modeling Ewing sarcoma tumors in vitro with 3D scaffolds. *Proc Natl Acad Sci U S A* **110**, 6500–6505.
[37] Lee SJ and Atala A (2013). Scaffold technologies for controlling cell behavior in tissue engineering. *Biomed Mater* **8**, 010201.
[38] Davies EJ, Dong M, Gutekunst M, Narhi K, van Zoggel HJ, Blom S, Nagaraj A, Metsalu T, Oswald E, and Erkens-Schulze S, et al (2015). Capturing complex tumour biology in vitro: histological and molecular characterisation of precision cut slices. *Sci Rep* **5**, 17187.
[39] Sachs N and Clevers H (2014). Organoid cultures for the analysis of cancer phenotypes. *Curr Opin Genet Dev* **24**, 68–73.
[40] Pickl M and Ries CH (2009). Comparison of 3D and 2D tumor models reveals enhanced HER2 activation in 3D associated with an increased response to trastuzumab. *Oncogene* **28**, 461–468.
[41] Howes AL, Richardson RD, Finlay D, and Vuori K (2014). 3-Dimensional culture systems for anti-cancer compound profiling and high-throughput screening reveal increases in EGFR inhibitor-mediated cytotoxicity compared to monolayer culture systems. *PLoS One* **9**, e108283.